PHYSICAL REVIEW A **73**, 041802(R) (2006)

Observation of multiple thresholds in the many-atom cavity QED microlaser

C. Fang-Yen,[1,*] C. C. Yu,[1] S. Ha,[1,†] W. Choi,[2] K. An,[2] R. R. Dasari,[1] and M. S. Feld[1]
[1]*G. R. Harrison Spectroscopy Laboratory, Massachusetts Institute of Technology, Cambridge, Massachusetts 02139, USA*
[2]*Department of Physics, Seoul National University, Seoul, Korea 151–742*
(Received 10 October 2005; published 20 April 2006)

We report the observation of multiple laser thresholds in the many-atom cavity QED microlaser. Traveling-wave coupling and a supersonic atom beam are used to create a well-defined atom-cavity interaction. Multiple thresholds are observed as jumps in photon number due to oscillatory gain. Although the number of intracavity atoms is large, up to $N \sim 10^3$, the dynamics of the microlaser agree with a single-atom theory. This agreement is supported by quantum trajectory simulations of a many-atom microlaser and a semiclassical microlaser theory. We discuss the relation of the microlaser with the micromaser and conventional lasers.

DOI: 10.1103/PhysRevA.73.041802 PACS number(s): 42.50.Pq, 42.55.−f

The most fundamental model of light-matter interaction at the atomic level consists of a two-level atom coupled to a single mode of the electromagnetic field, e.g., in an optical resonator. For an atom-cavity coupling strength greater than the decay rates of an atom and cavity ($g \gg \Gamma_c, \Gamma_a$), an excited atom exchanges energy coherently with the cavity (Rabi oscillation) [1].

Atom-resonator interaction is also the domain of laser physics; therefore, it may be somewhat surprising that most descriptions of laser operation use an *incoherent* model involving population densities and Einstein *A* and *B* coefficients. Such a model applies due to gain medium broadening, laser field nonuniformity, and other statistical effects [2].

The microlaser is a laser in which coherent Rabi oscillation is explicitly reflected in the dynamics of the laser. A controlled atom-cavity interaction and absence of strong statistical averaging leads to behavior foreign to conventional lasers. In this letter, we report the most dramatic of these effects; the existence of multiple laser thresholds.

The microlaser is the optical analogue of the micromaser [3], in which a similar bistable behavior has been observed for a single atom in the cavity [4]. The most significant differences between the two experiments are: (i) A large number of atoms is present, (ii) optical frequencies allow direct detection of generated light, and (iii) the number of thermal photons at optical frequencies is negligible.

An earlier version of the microlaser experiment [5] was shown to exhibit laser action with an intracavity atom number *N* on the order of 1. In the current setup, $N \gg 1$; remarkably, the many-atom system exhibits very similar behavior to that predicted from a single-atom theory. This is supported by quantum trajectory simulations [6] and may be explained by a semiclassical theory [7]. In addition, a theoretical study of a mesoscopic system of Rydberg atoms in a cavity driven by a external field [8] demonstrated bistability and multistability via a related mechanism.

The experiment is illustrated in Fig. 1. A supersonic beam of ^{138}Ba atoms passes through the TEM_{00} mode of a high-finesse optical cavity (symmetric near-planar cavity, mirror separation $L \approx 0.94$ mm, mirror radius of curvature $r_0 = 10$ cm, finesse $F \approx 9.0 \times 10^5$.) The mirror separation and finesse were determined by measurement of transverse mode spacing and cavity ringdown decay time. The background pressure in the vacuum chamber is less than 10^{-6} Torr. Prior to entering the cavity mode, each atom is excited by a continuous-wave pump laser (Coherent 899-21 Ti:Sapphire ring laser) locked to the $^1S_0 \leftrightarrow {}^3P_1$ transition ($\lambda = 791.1$ nm, linewidth $\Gamma_a \approx 50$ kHz) as described in [9]. The pump beam is focused by a cylindrical lens to a roughly 50 μm $\times$ 500 μm elliptical Gaussian beam centered approximately 150 μm from the cavity axis. This distance between pump and cavity mode assures that the pump beam does not overlap the cavity, while minimizing the effect of atomic decay between the pump and cavity. The total decay rate from the $^3P_1$ excited state corresponds to a decay length ≈ 1.3 mm for an atom velocity of 815 m/s. The cavity spacing is adjusted by a piezoelectric modulator (PZT) to be close to resonance with the $^1S_0 \leftrightarrow {}^3P_1$ transition by monitoring a $\lambda = 791.1$ nm probe beam through the cavity. The pump beam polarization direction is set perpendicular to the cavity axis to ensure

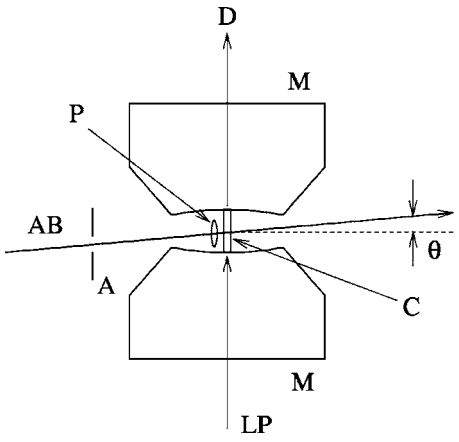

FIG. 1. Schematic of cavity QED microlaser. M: Cavity mirrors, C: Cavity mode, AB: Atomic beam from oven, A: Collimating aperture, P: Pump field (into page), θ: Cavity tilt angle, LP: Locking probe beam. Dashed line is normal to cavity axis.

*Electronic address: minwah@mit.edu
†Now at: Department of Physics, University of Wisconsin, Madison, WI 53706.

maximum coupling. A magnetic field of $\approx$150 Gauss oriented parallel to the pump beam polarization ensures that only $m=0 \leftrightarrow m=0$ transitions occur.

To measure the state of atoms which have passed through the pump beam, we monitor fluorescence of the atoms in the focused beam of a dye laser tuned to the $^1S_0 \leftrightarrow {}^1P_1$, $\lambda=553.5$ nm transition. The atoms were found to follow an adiabatic inversion process due to a Doppler frequency chirp from pump beam defocus. The effect is similar to that described in [10]. Incomplete inversion of the atoms by the pump beam is accounted for by defining an effective atom number $N_{\text{eff}} \equiv N(\rho_{ee}-\rho_{gg})$, where ρ_{ee}, ρ_{gg} are the excited and ground state populations of the atoms entering the cavity. For the data presented here, $\rho_{ee}-\rho_{gg} \approx 0.70$.

The atom-cavity interaction time $t_{\text{int}}=\sqrt{\pi} w_m/v_0 \approx 0.10$ μs, with $w_m \approx 41$ μm as the mode waist of the cavity and central atom velocity v_0. In order to observe multiple thresholds, a well-defined atom-cavity interaction is essential, requiring a redesign of the earlier system [5].

Uniform atom-cavity interaction is achieved via control of atom-cavity coupling g and interaction time t_{int}. The rapid spatial variation in coupling due to cavity standing wave is eliminated by introducing a small tilt of the atomic beam relative to the normal to the cavity axis (cf. [11]). In this configuration, the microlaser exhibits two Doppler-shifted resonances approximately centered at cavity frequencies $\omega_a \pm k v_0 \theta$ where ω_a is the atom resonance frequency.

The peak traveling-wave atom-cavity coupling is given by $g_0=(1/2)\mu\hbar\sqrt{\omega_a/2\epsilon_0 V} \approx 190$ kHz, where $V=\pi L w_0^2/4$ is the cavity mode volume and μ is the dipole matrix element. Note that this expression for g_0 reflects a factor of 2 reduction in the peak coupling relative to the standing wave value.

The atom beam is restricted to the center of the Gaussian mode by a 25 μm $\times$ 250 μm rectangular aperture located approximately 3 mm from the cavity axis. The aperture is translated and rotated in order to overlap the cavity axis as closely as possible. The resulting total atom-to-atom variation in peak coupling g is estimated to be $\approx$10%.

To ensure uniform atom-cavity interaction times, a supersonic atomic beam with narrow velocity distribution is used. The beam oven is similar to that of [12] and consists of a barium-filled resistively heated tantalum tube with a 250 micron diameter nozzle. The distance between the oven and cavity is 45 cm. The longitudinal velocity distribution was measured via a Doppler fluorescence measurement to be maximum at $v_0 \approx 815$ m/s and have a width of $\Delta v_{\text{FWHM}} \approx 100$ m/s. A total full width at half maximum (FWHM) variation in $g t_{\text{int}}$ of approximately 15% is achieved. Atomic density in the cavity is modulated by a translating knife edge approximately halfway between the oven and beam aperture.

A heuristic rate equation for the microlaser may be obtained by equating the photon gain and loss per atom transit:

$$P_{\text{emit}}(n) = \frac{\Gamma_c t_{\text{int}} n}{N_{\text{eff}}}, \tag{1}$$

where

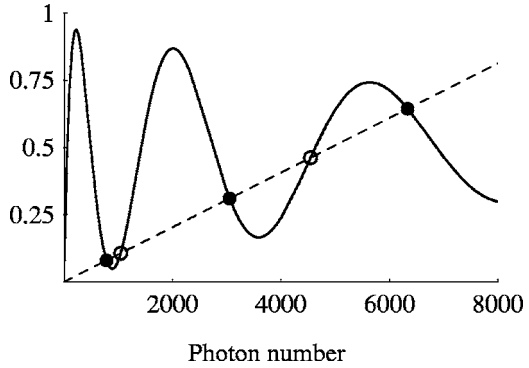

FIG. 2. Gain (solid line) and loss (dashed line) per atom transit in the rate equation analysis [left and right sides of Eq. (1), respectively] including effects of velocity distribution, nonuniform coupling, and detuning, with $N_{\text{eff}}=1000$. Closed circles: Stable solutions. Open circles: Unstable solutions.

$$P_{\text{emit}}(n) = \int dg f(g) \int dt_{\text{int}} h(t_{\text{int}}) \sin^2(\sqrt{n+1} g t_{\text{int}})$$

is the average emission probability for an atom and n is the number of photons in the cavity. The integrals over g and t_{int} with respective weighting functions $f(g)$ and $h(t_{\text{int}})$ reflect the distributions in these values. (An analogous stochastic averaging is justified in the appendix of [13].)

The rate equation is expressed graphically in Fig. 2. Damping in the oscillatory gain results from averaging over g and t_{int}. A solution n' of Eq. (1) is stable if $\partial/\partial n(P_{\text{emit}}(n) - \Gamma_c t_{\text{int}} n/N_{\text{eff}})|_{n'} < 0$. For a sufficiently large atom number, there exist more than one stable solution.

We now describe two experiments to observe multiple thresholds, the transitions between solutions of Eq. (1). In the first experiment, the microlaser cavity was locked on resonance ($\omega_{\text{cav}}=\omega_a+k v_0 \theta$) and the microlaser emission measured as a function of atom density. The cavity was chopped between data collection and locking on resonance with the atoms. Locking was performed with a 791 nm probe beam tuned to $\omega_a+k v_0 \theta$ via acousto-optic modulators and aligned with the TEM_{00} mode of the cavity. The cavity transmission was monitored by an avalanche photodiode and a feedback loop controlled the cavity PZT voltage to hold the cavity at resonance. Photons exiting the cavity were incident on a cooled photomultiplier tube and pulses are recorded by a photon counter.

We collected two sets of data in which: (i) The cavity photon number was allowed to develop from an initially empty cavity ($n=0$), and (ii) the cavity was seeded with a large ($n \sim 10^7$) number of photons by a laser pulse provided by the cavity locking probe beam. In both cases, the microlaser emission was observed for 100 ms.

Results from the cavity locking experiment are shown in Fig. 3. The solid line represents the solution to Eq. (1) and is composed of two branches for the range of N_{eff} shown. The first (lower) and second (upper) branches correspond to the first and second Rabi oscillations of Fig. 2. The lower half of the second branch (the portion of the line with a negative slope in this figure) is unstable.

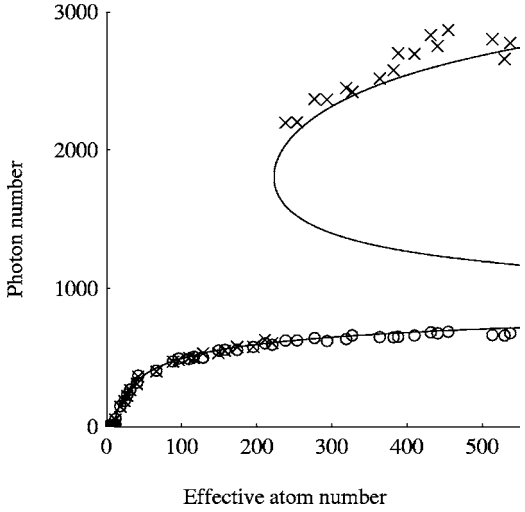

FIG. 3. Photon number n versus effective atom number N_{eff} for cavity locking experiment. Circles (○): "Unseeded" data; Crosses (×): "Seeded" data. Solid line: Rate equation model, solution of Eq. (1) for experimental parameters.

The intracavity atom number was determined by measuring fluorescence at ${}^1S_0 \leftrightarrow {}^1P_1$, $\lambda = 553.5$ nm with an imaging system and charge coupled device (CCD) camera. Uncertainties in cavity transmission, optical reflection coefficients, and CCD quantum efficiency make it difficult to measure the absolute density accurately. A fit to the experimental data was used to obtain a scale factor. A fitting parameter is close to the value expected from fluorescence measurements. The number of photons in the cavity is similarly estimated by considering the cavity parameters, losses in the optics, and detector quantum efficiency. In both cases, the fitting parameters were within ±50% of expected values.

The unseeded results are in good agreement with the first solution branch. The seeded results agree with the first branch for densities up to the onset of bistability at $N_{\mathrm{eff}} \approx 240$; above this point, the results agree with the second branch.

A calculation for steady-state average photon number using the single-atom micromaser theory of Filipowicz *et al.* [13] predicts a sharp transition between the first and second branches in at $N_{\mathrm{eff}}^0 \approx 415$. No such transition was observed, apparently due to very long metastable lifetimes in the picture of the Fokker-Planck analysis of [13], due to the large photon number.

In the second experiment, the cavity detuning $\Delta_{\mathrm{cav}} = \omega_{\mathrm{cav}} - \omega_a$ is varied for constant atom density. Data for the detuning curves for a range of atom densities are shown in Fig. 4. The solid and dashed lines represent scans in the positive and negative detuning directions, respectively.

The two-peaked structure is due to two traveling-wave resonances of the tilted cavity. The Doppler splitting was measured to be about 27.1 MHz, corresponding to a cavity tilt angle $\theta \approx 13$ mrad.

As the density is increased, the two resonances broaden and increase in amplitude. For $N_{\mathrm{eff}} \approx 630$, the second threshold appears as a "spike" near the peak of each resonance, and at $N_{\mathrm{eff}} \approx 725$, a jump to a third branch appears.

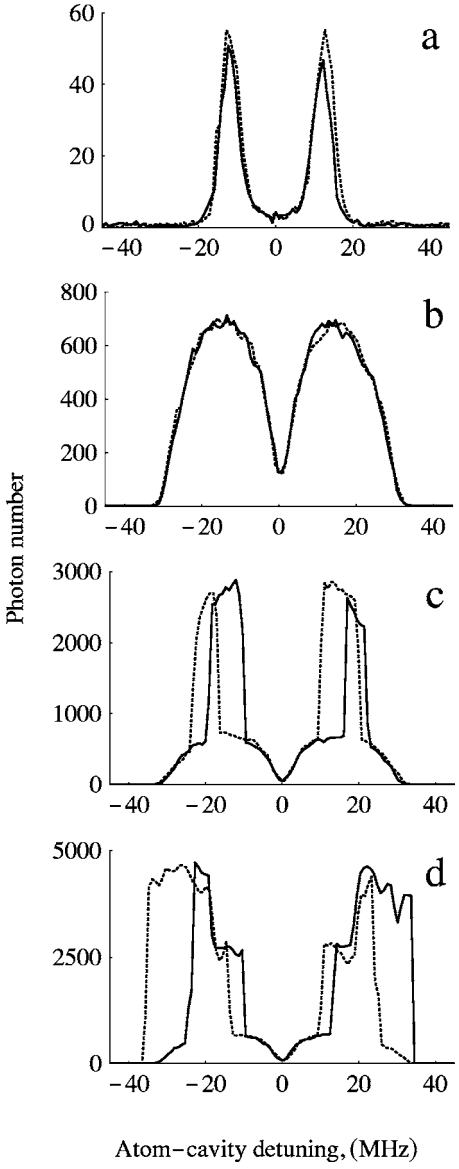

FIG. 4. Cavity tuning line shapes. Estimated photon number n versus atom-cavity detuning Δ_{cav}. Solid lines, positive frequency scan. Dashed lines, negative frequency scan. Estimated effective intracavity atoms: (a) $N_{\mathrm{eff}} = 18$, (b) $N_{\mathrm{eff}} = 526$, (c) $N_{\mathrm{eff}} = 657$, and (d) $N_{\mathrm{eff}} = 755$.

The detuning line shapes display strong asymmetry and hysteresis for atom numbers above the second threshold. For densities in which sudden jumps occur, each traveling-wave resonance of the cavity scanning line shapes is highly asymmetric and shows hysteresis as a function of scan direction. This is most likely due to interactions with the two Doppler-shifted fields at $\omega_a \pm k v_0 \theta$. For the general case in which neither field is dominant, the atoms experience a complex bichromatic interaction with these two fields. A simple model [14] has been shown to qualitatively describe the line shape asymmetry and hysteresis observed here. More detailed quantitative descriptions are in progress.

To examine the application of single-atom theory to our many-atom microlaser, a semiclassical theory [7] of the microlaser analogous to the Lamb theory of the conventional

laser [15] has been developed. In the case of monochromatic field and zero atom-cavity detuning, the semiclassical theory reduces to the rate equation model. This provides a more rigorous justification for Eq. (1).

We have also performed quantum trajectory simulations of a microlaser with up to five intracavity atoms [6]. The many-atom microlaser was shown to be in close agreement with the predictions from a single-atom theory [13], with a perturbation in the width of the photon number distribution due to cavity decay during the interaction time.

The connection between the microlaser with the conventional laser may be illustrated by considering the effect of increased variation in gt_{int}. For simplicity, suppose $f(g) = \delta(g-g_0)$ and interaction times are distributed according to atom lifetime. The dimensionless gain is then $P_{\mathrm{emit}} = \tau_a^{-1}\int_0^\infty dt_{\mathrm{int}} \exp(-t/\tau_a)\sin^2(\sqrt{n+1}gt_{\mathrm{int}}) = 1/2\{[(n+1)g^2\tau_a^2]/[1+(n+1)g^2\tau_a^2]\}$. With Eq. (1), this expression describes a conventional saturable gain laser, which is monostable and linear above threshold.

In the microlaser, for any finite degree of broadening in gt_{int}, we have $P_{\mathrm{emit}}(n\to\infty) = 1/2$. Therefore, conventional laser behavior is recovered in the limit of large photon number.

In summary, the microlaser is shown to exhibit multistability due to coherent atom-cavity interaction, which in conventional lasers is hidden by spontaneous emission and other incoherent processes.

We have recently demonstrated that the microlaser field exhibits sub-Poisson photon statistics [16] even for hundreds of intracavity atoms. Measurement of the spectrum of microlaser emission [17] is also planned.

This research was supported by National Science Foundation Grant Nos. 9876974-PHY and 0111370-CHE. K. An was supported by a Korea Research Foundation Grant (KRF-2002-070-C00044). The authors thank J. Thomas of Duke University for assistance with the supersonic atom beam, and M. O. Scully for many helpful discussions.

[1] E. T. Jaynes and F. W. Cummings, Proc. IEEE **51**, 89 (1963).
[2] M. O. Scully and S. Zubairy, *Quantum Optics* (Cambridge U.P., Cambridge, UK, 1997).
[3] D. Meschede, H. Walther, and G. Muller, Phys. Rev. Lett. **54**, 551 (1985).
[4] O. Benson, G. Raithel, and H. Walther, Phys. Rev. Lett. **72**, 3506 (1994).
[5] K. An, J. J. Childs, R. R. Dasari, and M. S. Feld, Phys. Rev. Lett. **73**, 3375 (1994).
[6] C. Fang-Yen, Opt. Commun. (in press).
[7] K. An, J. Korean Phys. Soc. **42**, 4 (2004).
[8] F. Casagrande, L. A. Lugiato, W. Lange, and H. Walther, Phys. Rev. A **48**, 790 (1993).
[9] K. An, Appl. Phys. Lett. **66**, 24 (1995).
[10] J. P. C. Kroon, H. A. J. Senhorst, H. C. W. Beijerinck, B. J. Verhaar, and N. F. Verster, Phys. Rev. A **31**, 3724 (1985).
[11] K. An, R. R. Dasari, and M. S. Feld, Opt. Lett. **22**, 1500 (1997).
[12] K. D. Stokes, C. Schnurr, J. Gardner, M. Marable, S. Shaw, M. Goforth, D. E. Holmgren, and J. Thomas, Opt. Lett. **14**, 1324 (1989).
[13] P. Filipowicz, J. Javanainen, and P. Meystre, Phys. Rev. A **34**, 3077 (1986).
[14] C. Fang-Yen, Ph.D. thesis, Massachusetts Institute of Technology, 2002.
[15] W. Lamb, Phys. Rev. **134**, A1429 (1964).
[16] W. Choi, J. Lee, K. An, C. Fang-Yen, R. R. Dasari, and M. S. Feld, Phys. Rev. Lett. **96**, 093603 (2006).
[17] M. O. Scully, H. Walther, G. S. Agarwal, T. Quang, and W. Schleich, Phys. Rev. A **44**, 5992 (1991).